Proceedings of the 4th International Conference on Functional Materials and Civil Engineering
DOI: 10.54254/2755-2721/2026.38709

MATLAB/Simulink Based Steady-State Power Flow Analysis and Voltage Characteristics Study of a Microgrid

Xiaoying Zhang

College of Information and Intelligence Engineering, Zhejiang Wanli University, Ningbo, China
wanlian62059@gmail.com

Abstract. Photovoltaic (PV) generation changes power flows and voltage profiles in grid-connected microgrids. This study examines these effects using the Baran–Wu IEEE 33-Bus Radial Distribution System under balanced operation at 50 Hz. A single PV unit is modeled as a constant-PQ source with zero reactive power. A current-based forward/backward sweep algorithm is implemented in MATLAB for eleven operating cases covering PV capacity, connection location, and load level. Two cases are checked independently using the MATPOWER Newton–Raphson solver, and four are verified using a three-phase Simscape Electrical network. At rated load, connecting 0.50 MW at bus 18 raises the minimum voltage from 0.91309 to 0.92451 pu and reduces total active power loss from 202.68 to 153.42 kW. Across the sampled capacities, losses initially decrease and then increase, with local reverse power flow occurring in some branches. Changing the connection location redistributes voltage improvements, whereas increased loading deepens voltage drops and increases losses. The maximum voltage difference between MATLAB and Simulink is below 5×10^{-10} pu. The results support steady-state comparisons of PV connection schemes under the specified network and constant-power assumptions.

Keywords: grid-connected microgrid, photovoltaic generation, forward/backward sweep, voltage profile

1. Introduction

Distributed generation supplies electricity within distribution networks or near end users [1]. In grid-connected microgrids, photovoltaic (PV) generation supplies local demand and changes upstream line currents, voltage drops, and bus voltages. Reverse power flow can occur when local generation exceeds downstream demand. Voltage changes depend on power flow direction, whereas losses depend on current magnitude; a higher voltage at the connection bus therefore does not necessarily imply lower total system losses.

Previous studies have examined source-bus representation and power flow control in AC/DC microgrids [2], distributed power flow calculation and optimization in hybrid microgrids [3], and source and load uncertainty through multi-factor feature fusion [4]. These studies inform equivalent source modeling and power flow analysis. Deterministic comparisons of a single PV unit require consistent network parameters when varying capacity, connection location, and load level; one operating point cannot capture their combined effects.

© 2026 The Authors. This is an open access article distributed under the terms of the Creative Commons Attribution License 4.0 (https://creativecommons.org/licenses/by/4.0/).

DOI: 10.54254/2755-2721/2026.38709

PV capacity determines the fraction of demand supplied locally, the connection location determines the affected supply paths, and the load level changes net demand at fixed PV output. Evaluating these factors separately helps identify weak buses and explain local reverse power flow and loss changes. Screening candidate schemes therefore requires both local voltage information and system-level loss metrics, rather than judging performance solely from the voltage at the PV connection bus.

This study develops a steady-state equivalent of a grid-connected AC microgrid with one PV unit using the IEEE 33-Bus Radial Distribution System. A current-based forward/backward sweep algorithm compares voltage profiles and active power losses across eleven operating cases. Selected cases are checked with an independent power flow solver and a Simulink physical network. Branch power flows explain how local voltage improvement relates to total system loss. The analysis supports preliminary comparison of PV connection schemes under consistent network assumptions, linking the numerical results to the supply paths and loading conditions that produce them.

2. Modeling of grid-connected microgrid and steady-state power flow method

2.1. Network structure and modeling assumptions

The network follows the Baran–Wu IEEE 33-Bus Radial Distribution System [5], with 32 closed radial branches, loads at buses 2–33, and one PV source modeled as a PQ bus. Bus 1 serves as both the point of common coupling (PCC) and the slack bus. An ideal three-phase source represents the external grid, providing voltage and frequency references of $1\angle 0°$ pu and 50 Hz. Normally open tie branches and external grid internals are excluded.

The external grid supplies remaining net demand and line losses through the PCC. In the location study, only the PV connection bus changes; the PCC remains at bus 1. The analysis assumes balanced three-phase operation at the fundamental frequency, with fixed frequency and topology. The PV unit provides neither voltage regulation nor frequency support. Islanding transitions and post-disturbance dynamic stability are outside the study's scope.

2.2. Steady-state models of lines, loads, and photovoltaic generation

The network follows the Baran–Wu IEEE 33-Bus Radial Distribution System [5], with 32 closed radial branches, loads at buses 2–33, and one PV source modeled as a PQ bus. Bus 1 serves as both the point of common coupling (PCC) and the slack bus. An ideal three-phase source represents the external grid, providing voltage and frequency references of $1\angle 0°$ pu and 50 Hz. Normally open tie branches and external grid internals are excluded.

The external grid supplies remaining net demand and line losses through the PCC. In the location study, only the PV connection bus changes; the PCC remains at bus 1. The analysis assumes balanced three-phase operation at the fundamental frequency, with fixed frequency and topology. The PV unit provides neither voltage regulation nor frequency support. Islanding transitions and post-disturbance dynamic stability are outside the study's scope.

$$S_{i,net} = \lambda S_{i,d} - S_{i,pv} \tag{1}$$

Net active consumption can be negative: the 90 kW load at bus 18 with 0.50 MW of PV gives −410 kW net active demand. Retaining this sign represents reverse power flow directly in the

DOI: 10.54254/2755-2721/2026.38709

network solution. The PQ equivalent describes grid-side power at specified output and excludes internal PV energy conversion.

2.3. Current-based forward/backward sweep power flow algorithm

The upstream–downstream structure of a radial network permits branch-current accumulation and recursive voltage updates [6]. These topology-based current–voltage relationships also underpin other distribution power flow methods [7]. The current-based forward/backward sweep starts from a flat $1\angle 0°$ pu profile. At iteration k, the current bus voltage estimate gives the net load current:

$$I_i^{(k)}=\left(\frac{S_{i,net}}{V_i^{(k)}}\right)^* \tag{2}$$

The backward sweep processes branches from terminal buses toward the PCC. Branch i–j carries the sum of bus j's net load current and currents in its outgoing downstream branches. The forward sweep then updates voltages from the PCC toward terminal buses using line impedances. Here, C(j) denotes buses immediately downstream of j:

$$I_{ij}^{(k)}=I_j^{(k)}+\sum I_{jm}^{(k)},m\in C(j) \tag{3}$$

$$V_j^{(k+1)}=V_i^{(k+1)}-z_{ij}I_{ij}^{(k)} \tag{4}$$

Iteration stops when the maximum bus voltage change is below 10^{-8} pu, subject to a limit of 100 iterations. Branch currents are recalculated from final voltage differences, and sending-end powers, receiving-end powers, and losses use the same converged solution. The superscript * denotes complex conjugation. Branch sending-end complex power and complex loss are

$$S_{ij}=V_iI_{ij}^*,\ \Delta S_{ij}=z_{ij}|I_{ij}|^2 \tag{5}$$

2.4. Voltage and power flow evaluation indicators

Evaluation metrics include voltage magnitudes and phase angles, minimum voltage and its location, maximum voltage, branch sending-end and receiving-end active and reactive powers, and total active and reactive losses. Sending-end power is positive from the upstream to the downstream bus. Branch losses sum the powers entering both line ends and are converted from per unit using the power base.

The interval 0.95–1.05 pu provides a reference for comparing voltage profiles. Counts below and above these limits describe violations, not probabilities. Power balance compares PCC input plus PV generation with total load plus losses. Signed flows and voltage violations distinguish local voltage improvement from overall system performance.

The loss metric represents a steady-state operating point. Without considering generation duration, a case's power loss reduction cannot be interpreted directly as reduced annual energy losses.

DOI: 10.54254/2755-2721/2026.38709

3. Establishment of MATLAB and simulink models and verification methods

3.1. IEEE 33-Bus case data and base parameters

Standard branch resistances and reactances, bus active and reactive demands, and bus numbering are checked against MATPOWER case33bw. Table 1 lists the 3.715 MW + j2.300 Mvar base load and MATLAB bases: 12.66 kV line-to-line RMS voltage and 10 MVA three-phase power. The impedance base is V^2/S.

Table 1. IEEE 33-Bus test system and per-unit bases

Parameter	Value	Definition
Buses / Closed Branches	33 / 32	Radial Topology
Total Base Load	3.715 MW + j2.300 Mvar	Sum of Bus Loads
Voltage Base	12.66 kV	Line-to-Line RMS Voltage
Power Base	10 MVA	Three-Phase Total Power
Impedance Base	16.02756 Ω	V_{base}^2 / Sbase
Frequency	50 Hz	Balanced Three-Phase Fundamental

Line impedances in Ω and bus demands in kW/kvar are converted to MATLAB per-unit quantities without mixing MATPOWER's own baseMVA convention. Calculations repeated at 1 MVA and 100 MVA give consistent results after conversion back to physical units. Figure 1 identifies candidate connection locations; each case contains only one equivalent PV source.

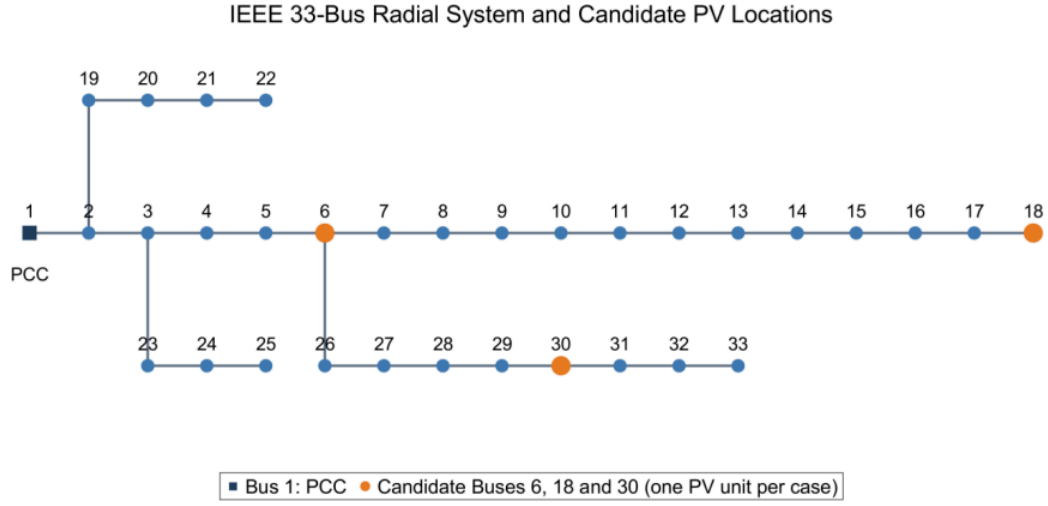


Figure 1. IEEE 33-Bus Radial Distribution System and candidate PV locations

3.2. MATLAB power flow calculation and operating cases

MATLAB R2024b performs unit conversion, topology ordering, forward/backward sweeps, branch power calculation, and plotting. Cases share the Section 3.1 parameters and fixed PCC voltage, frequency, and PV reactive power; comparison groups vary one factor at a time.

At rated load, PV capacity at bus 18 takes values of 0, 0.25, 0.50, 0.75, and 1.00 MW; location comparisons use 0.50 MW at buses 6, 18, and 30. Load multipliers of 0.8, 1.0, and 1.2 scale active and reactive demand proportionally, comparing no PV with 0.50 MW at bus 18.

DOI: 10.54254/2755-2721/2026.38709

Table 2 contains 11 distinct cases after duplicate combinations are removed. Each represents fixed-output steady state, not an irradiance time series.

All cases converge in 7–8 iterations with finite results. The maximum complex power balance residual is within 2.17×10^{-5} kVA.

Table 2. Minimum voltage and total active power loss for each case

Case	PV Bus	PV Power / MW	Load Multiplier	V min / pu	Bus at Vmin	Active Loss / kW
C1	—	0.00	1.0	0.91309	18	202.68
C2	18	0.25	1.0	0.92067	33	172.22
C3	18	0.50	1.0	0.92451	33	153.42
C4	18	0.75	1.0	0.92813	33	144.96
C5	18	1.00	1.0	0.93157	33	145.79
C6	6	0.50	1.0	0.92075	18	167.08
C7	30	0.50	1.0	0.92100	18	154.92
C8	—	0.00	0.8	0.93163	18	125.80
C9	18	0.50	0.8	0.94192	33	92.36
C10	—	0.00	1.2	0.89384	18	301.45
C11	18	0.50	1.2	0.90647	33	234.48

3.3. Establishment of simulink microgrid model

Simulink represents the same three-phase system with an external grid, 32 series R–L lines, 32 constant-power loads, and one PV PQ source. Line inductance is $L = X/(2\pi f)$; load and PV inputs are total three-phase powers. Measurements cover all bus voltage magnitudes and angles, and active and reactive powers in branches 1–2, 17–18, and 29–30.

Simscape frequency-and-time mode initializes the network at sinusoidal steady state [8]. The MATLAB solution is not supplied to the physical network or its Scopes. Each simulation runs for 1 s, with measurements evaluated over 0.8–1.0 s. These remain steady, making longer runs unnecessary for the specified operating points. The default case uses 0.50 MW at bus 18; other selected cases retain the same network.

3.4. Comparison method between power flow calculation and simulation results

The Newton–Raphson solver in MATPOWER 8.1 independently checks operation without PV and with 0.50 MW at bus 18 [9]. Maximum differences are within 4.14×10^{-10} pu for bus voltage, below 1.14×10^{-5} kW for PCC active power, and below 1.41×10^{-6} kW for total active power loss. These comparisons support numerical consistency of the forward/backward sweep implementation.

Both platforms use per-unit line-to-line RMS voltage, total three-phase power, and positive flow from PCC to loads. Window averages, extrema, and peak-to-peak values are recorded; averages are compared with converged MATLAB results. The four validation cases cover the base condition, capacity variation, and location variation: no PV, 0.50 MW and 1.00 MW at bus 18, and 0.50 MW at bus 30 (C1, C3, C5, and C7).

DOI: 10.54254/2755-2721/2026.38709

4. Steady-state power flow and voltage characteristics analysis

4.1. Base case and comparison before and after photovoltaic connection

Without PV, the minimum voltage is 0.91309 pu at bus 18, the maximum is 1.00000 pu at the PCC, and total active power loss is 202.68 kW. With 0.50 MW at bus 18, its voltage reaches 0.95088 pu; the minimum shifts to bus 33 at 0.92451 pu. Figure 2 shows the strongest improvement near the connection bus, leaving a terminal bus on another feeder as the lowest-voltage location.

Total active power loss falls to 153.42 kW, a reduction of 24.30%. PCC active power falls from 3.91768 to 3.36842 MW, reflecting local generation and lower losses. Buses below 0.95 pu decrease from 21 to 15, so undervoltage persists. Profile points join in bus-number order; the transition from bus 18 to bus 19 does not represent a physical line connection.

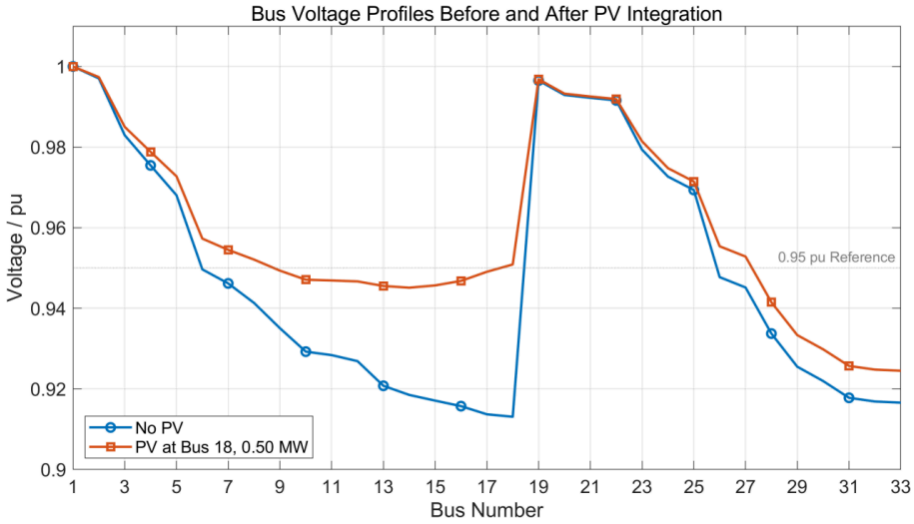


Figure 2. Bus voltage profiles before and after PV integration

4.2. Effect of photovoltaic connection capacity on voltage and network loss

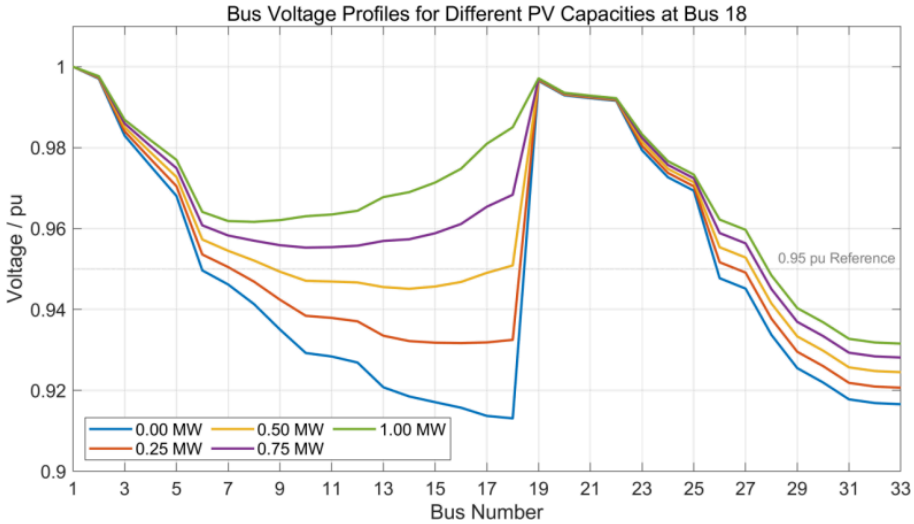


Figure 3. Bus voltage profiles under different PV capacities

DOI: 10.54254/2755-2721/2026.38709

Capacity and location jointly affect losses [10]. Figure 3 shows that increasing bus 18 output from 0 to 1.00 MW raises its voltage from 0.91309 to 0.98504 pu; the system minimum reaches 0.93157 pu. Maximum voltage remains 1 pu, with none above 1.05 pu.

Table 2 and Figure 4 show loss decreasing to 144.96 kW at 0.75 MW, then rising to 145.79 kW at 1.00 MW. The best sampled capacity does not establish a continuous global optimum.

At low to moderate capacities, local PV supply reduces upstream line currents and total active power loss. At higher capacities, stronger reverse flow increases current magnitudes and losses in some branches. Total loss rises when these increases outweigh reductions elsewhere. Branch 17–18, examined in Section 4.5, illustrates why continued voltage improvement can coexist with increasing losses.

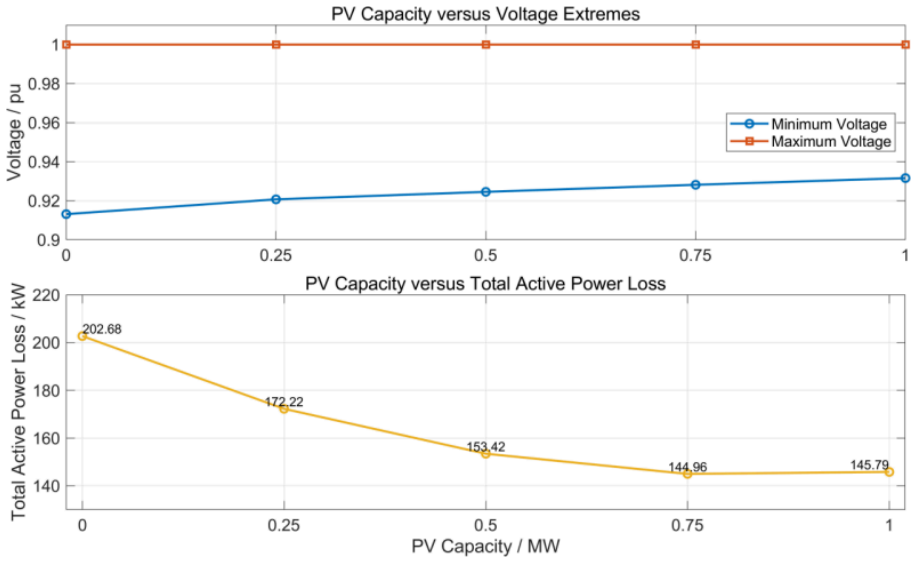


Figure 4. PV capacity versus voltage extremes and active power loss

4.3. Effect of photovoltaic connection location on voltage and network loss

Location determines the supply paths affected by generation, consistent with studies of how distributed generation location and size influence losses [11]. Table 2 compares 0.50 MW connections at buses 6, 18, and 30; Figure 5 shows their voltage profiles.

Bus 18 gives the highest system minimum voltage and lowest total active power loss among these candidates. Connection at bus 30 raises its voltage to 0.93948 pu, versus 0.92982 pu with PV at bus 18. Greater local voltage improvement therefore does not necessarily yield a higher system minimum. The comparison is limited to these candidate locations and does not establish globally optimal siting.

Bus 30's base reactive demand is 600 kvar, while PV reactive output is zero. PV reduces active power transmission along this feeder, but the grid still supplies its reactive demand. The feeder containing bus 18 continues to supply its own loads. Voltage improvements are therefore concentrated along the supply paths associated with each PV connection.

DOI: 10.54254/2755-2721/2026.38709

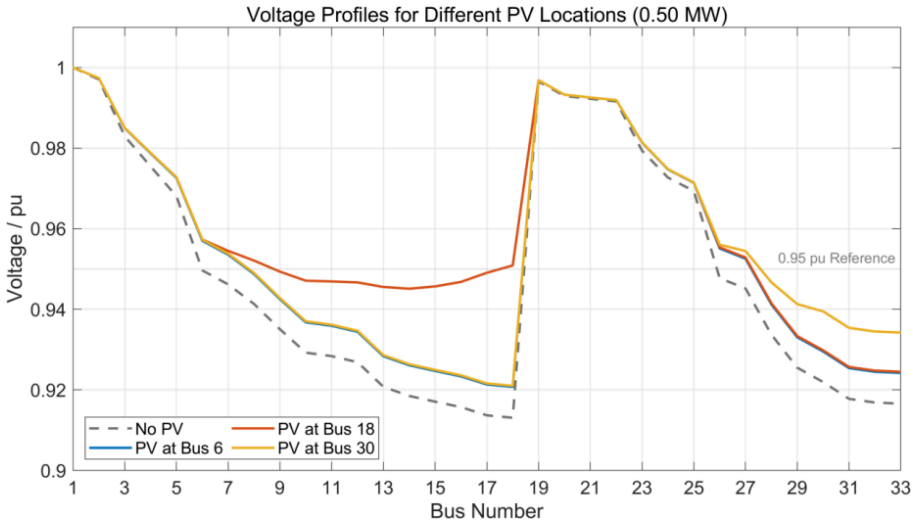


Figure 5. Voltage comparison for different PV connection locations

4.4. Voltage characteristics under different load levels

Table 2 and Figure 6 show that raising the load multiplier from 0.8 to 1.2 lowers minimum voltage and increases losses both with and without PV. Fixed 0.50 MW output reduces losses but cannot offset load-driven voltage decline.

Under heavy load, 21 buses remain below 0.95 pu with or without PV despite improved voltages. Violation counts miss improvements below the threshold and require interpretation alongside minimum voltage and the full profile.

Fixed 0.50 MW output supplies 16.82% of demand at load multiplier 0.8 but only 11.22% at 1.2. Constant-power loads draw more current at lower voltage, reinforcing terminal voltage drops and line losses under heavy loading.

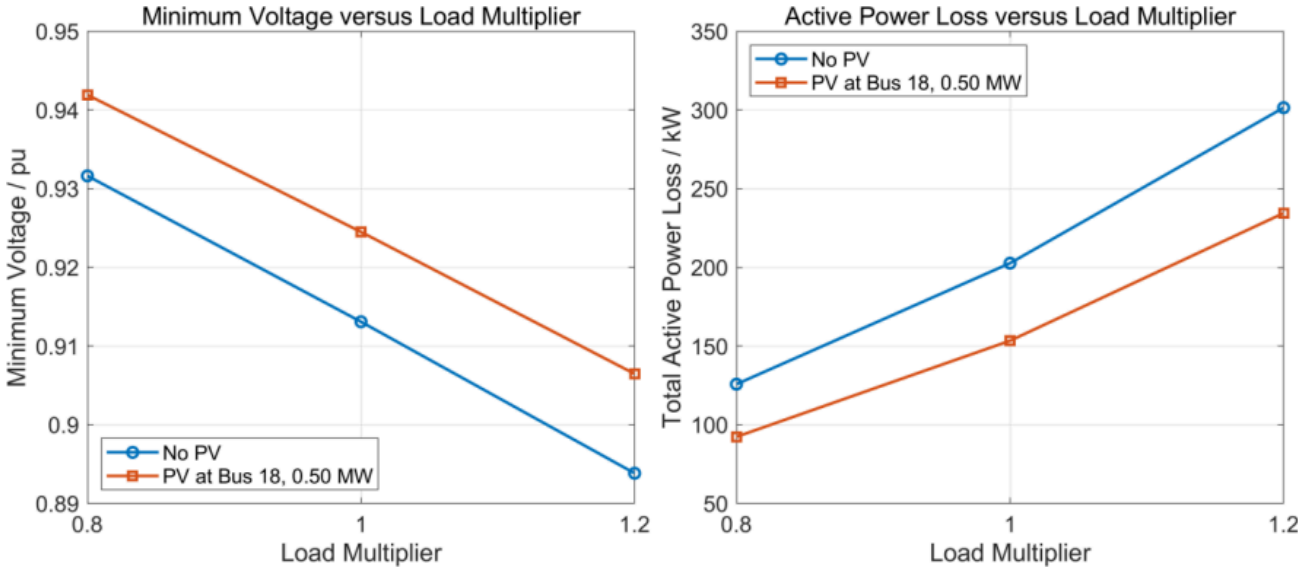


Figure 6. Minimum voltage and active power loss under different load levels

DOI: 10.54254/2755-2721/2026.38709

4.5. Mechanism of line power and network loss changes

Line voltage drop depends on impedance and transmitted power, whereas active power loss scales with squared current magnitude. At 0.50 MW, PV reduces active transmission in the main upstream lines but reverses terminal-branch flow. Sending-end power in branch 17–18 changes from 0.09005 to −0.40914 MW, and its active loss increases from 0.053 to 0.857 kW. Total system loss nevertheless decreases, demonstrating opposite local and system-wide changes.

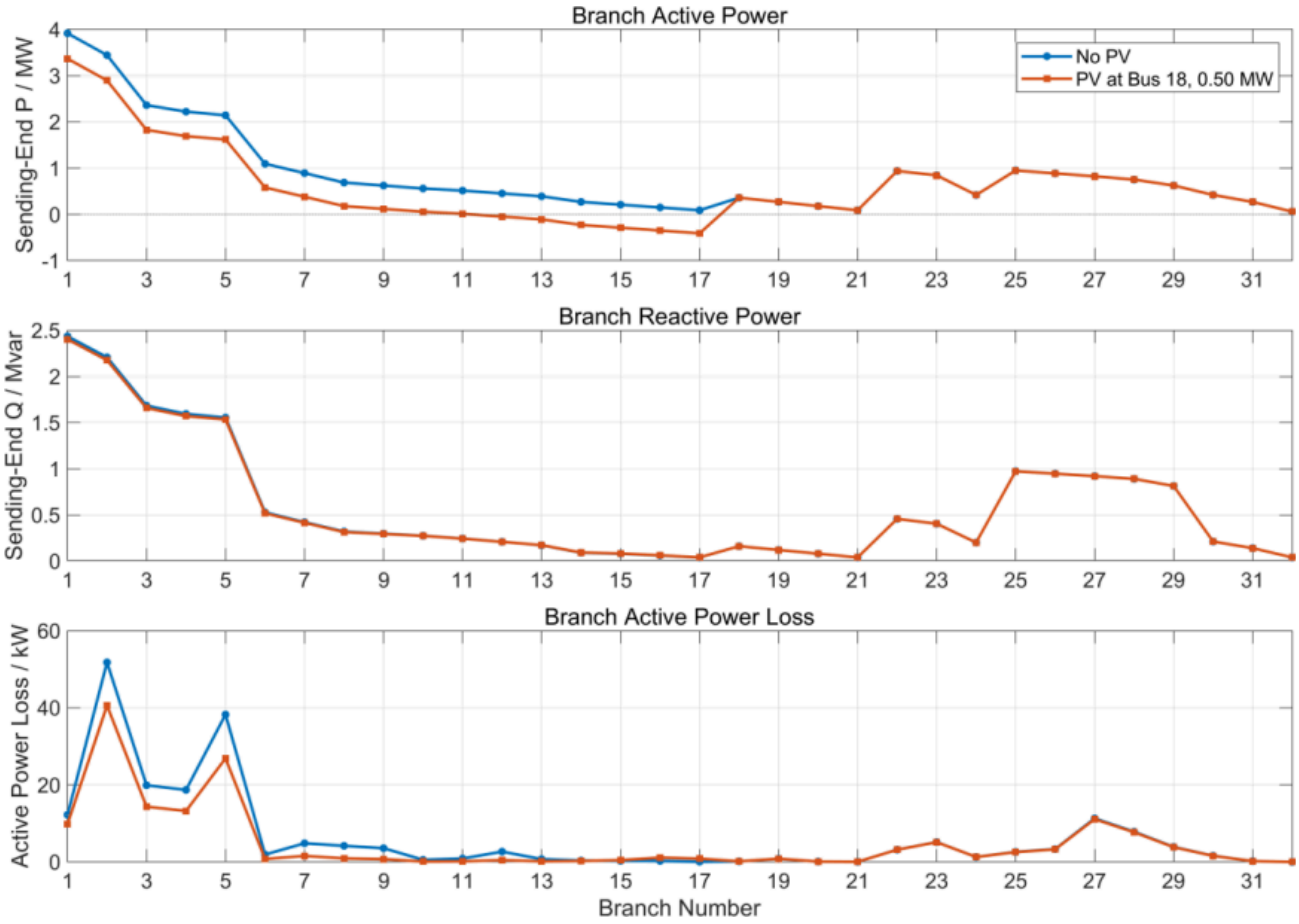


Figure 7. Branch power flow and active power loss

At 1.00 MW, branch 17–18 sending-end active power reaches −0.90609 MW and its loss rises to 3.905 kW. As capacity increases at rated load, reverse-flow branches reach 11, although the PCC continues to import power. With zero PV reactive output, changes in PCC reactive power mainly reflect line reactive losses rather than reactive compensation by the PV unit.

4.6. Simulation verification of typical steady-state cases

Using the comparison method in Section 3.4, all four physical-network cases complete 1 s runs with finite results. Window peak-to-peak variations stay below 1.0×10^{-14} pu for voltage and 1.0×10^{-13} MW or Mvar for power, consistent with steady-state initialization. MATLAB and Simulink curves overlap in Figure 8; Table 3 gives PCC active power and maximum differences.

Voltage differences are maxima across 33 buses; power differences are maxima across three measured branches. The largest voltage difference is 4.39×10^{-10} pu, and maximum relative power

DOI: 10.54254/2755-2721/2026.38709

difference is within 2.19 × 10^{-6}%. This agreement supports consistent steady-state models and unit conventions, without establishing fast-transient accuracy.

Table 3. Steady-state comparison between MATLAB and simulink

Case	Simulink PCC / MW	Maximum Voltage Error / pu	Maximum P Error / kW	Maximum Q Error / kvar
C1	3.917677	1.02e-10	2.95e-06	2.04e-06
C3	3.368417	4.13e-10	1.14e-05	7.65e-06
C5	2.860795	3.34e-11	5.94e-07	1.19e-06
C7	3.369925	4.39e-10	1.16e-05	7.82e-06

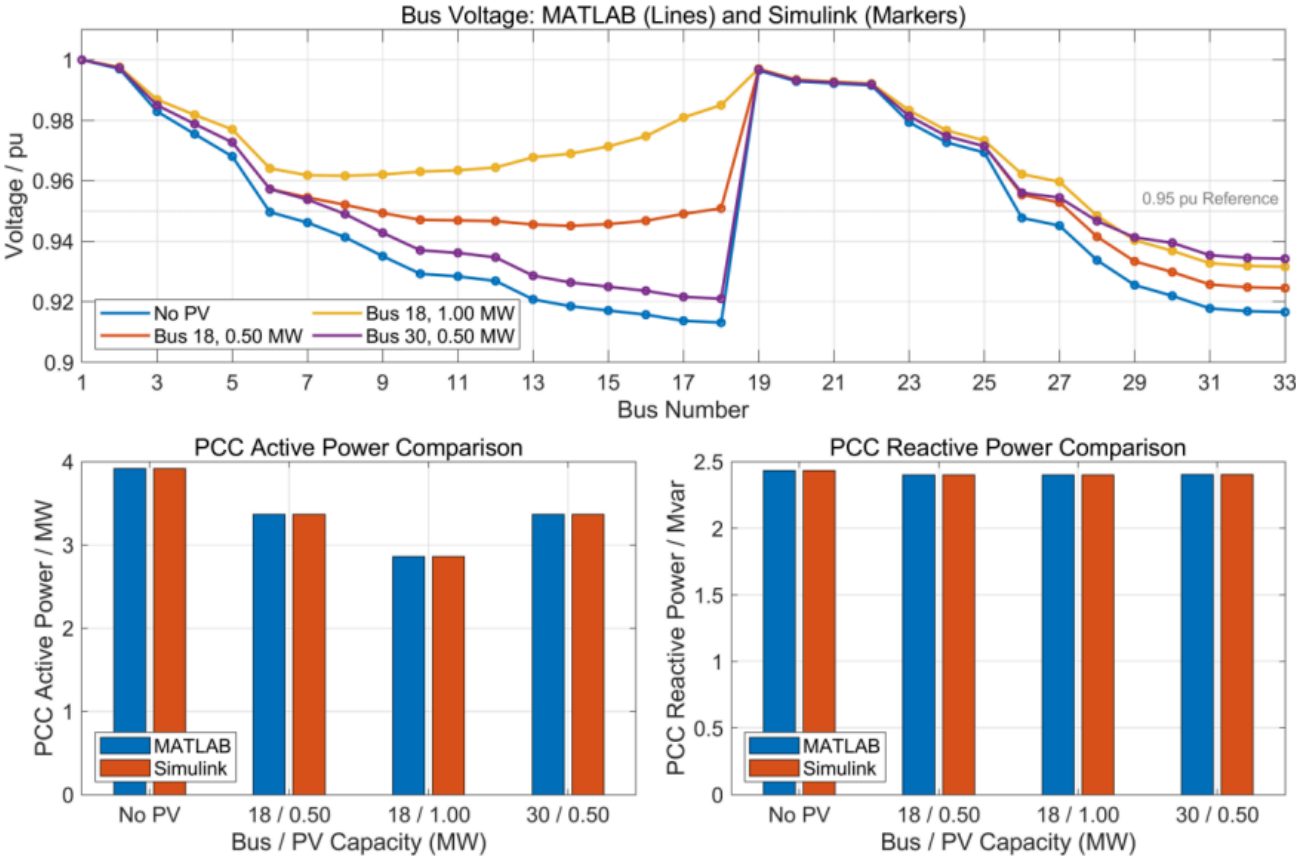


Figure 8. Comparison between MATLAB and simulink results

5. Conclusion

Current-based forward/backward sweep analysis of the IEEE 33-Bus Radial Distribution System shows how PV capacity, location, and loading affect a grid-connected microgrid. At rated load, 0.50 MW at bus 18 raises minimum voltage from 0.91309 to 0.92451 pu and reduces active power loss from 202.68 to 153.42 kW (24.30%), although some buses remain below 0.95 pu.

Voltage improves with capacity, but stronger reverse flows eventually raise total loss; 0.75 MW gives the lowest loss among the sampled capacities. Among the three 0.50 MW locations, connection at bus 18 gives the highest system minimum voltage and lowest total active power loss, whereas bus 30 provides greater local voltage improvement on its feeder.

DOI: 10.54254/2755-2721/2026.38709

Raising the load multiplier from 0.8 to 1.2 lowers voltage and increases losses with or without PV, so fixed output cannot offset load growth. The four MATLAB–Simulink comparisons give a maximum voltage difference of 4.39×10^{-10} pu and relative power difference below 1%, supporting consistent steady-state modeling.

Minimum voltage, branch flows, and total loss should therefore be assessed together when screening connection schemes. The findings apply to balanced three-phase operation with constant-power loads, fixed PV output, and the selected capacities and locations; they establish neither global optima nor dynamic stability. Further work could refine capacity increments and compare alternative load models within this framework.

References

[1] Ackermann, T., Andersson, G., & Söder, L. (2001). Distributed generation: A definition. *Electric Power Systems Research, 57*(3), 195–204. https://doi.org/10.1016/S0378-7796(01)00101-8.

[2] Kang, S. W. (2023). *Power flow control and power flow calculation of AC/DC microgrid*. Master's thesis, Shijiazhuang Tiedao University, Shijiazhuang. (In Chinese).

[3] Liu, Y. T. (2023). *Distributed power flow calculation and optimization methods for hybrid AC/DC microgrid*. Master's thesis, Shandong University, Jinan. (In Chinese).

[4] Feng, K. (2023). *Research on stochastic power flow calculation and optimization strategy of microgrid based on multi-factor feature fusion*. Master's thesis, North Minzu University, Yinchuan. (In Chinese).

[5] Baran, M. E., & Wu, F. F. (1989). Network reconfiguration in distribution systems for loss reduction and load balancing. *IEEE Transactions on Power Delivery, 4*(2), 1401–1407. https://doi.org/10.1109/61.25627.

[6] Shirmohammadi, D., Hong, H. W., Semlyen, A., & Luo, G. X. (1988). A compensation-based power flow method for weakly meshed distribution and transmission networks. *IEEE Transactions on Power Systems, 3*(2), 753–762. https://doi.org/10.1109/59.192932.

[7] Teng, J. H. (2003). A direct approach for distribution system load flow solutions. *IEEE Transactions on Power Delivery, 18*(3), 882–887. https://doi.org/10.1109/TPWRD.2003.813818.

[8] The MathWorks, Inc. (n.d.). Frequency and time simulation mode. *MATLAB and Simulink Documentation*. https://www.mathworks.com/help/simscape/ug/frequency-and-time-simulation.html. Accessed 7 September 2026.

[9] Zimmerman, R. D., Murillo-Sánchez, C. E., & Thomas, R. J. (2011). MATPOWER: Steady-state operations, planning, and analysis tools for power systems research and education. *IEEE Transactions on Power Systems, 26*(1), 12–19. https://doi.org/10.1109/TPWRS.2010.2051168.

[10] Acharya, N., Mahat, P., & Mithulananthan, N. (2006). An analytical approach for DG allocation in primary distribution network. *International Journal of Electrical Power & Energy Systems, 28*(10), 669–678. https://doi.org/10.1016/j.ijepes.2006.02.013.

[11] Muslimin, Z., Suyuti, A., Palantei, E., Indrabayu, & Gunadin, I. C. (2022). Analysis of distributed generation integration effect on active power losses in distribution networks. *International Journal of Electrical and Electronic Engineering & Telecommunications, 11*(2), 102–108. https://doi.org/10.18178/ijeetc.11.2.102-108.